REAL-TIME POSE ESTIMATION USING TREE STRUCTURES BUILT FROM SKELETONISED VOLUME SEQUENCES

Rune Havnung Bakken[1] and Adrian Hilton[2]
[1]*Faculty of Informatics and e-Learning, Sør-Trøndelag University College, Trondheim, Norway*
[2]*Centre for Vision, Speech and Signal Processing, University of Surrey, Guildford, U.K.*

Keywords: Human Motion, Pose Estimation, Real-time.

Abstract: Pose estimation in the context of human motion analysis is the process of approximating the body configuration in each frame of a motion sequence. We propose a novel pose estimation method based on constructing tree structures from skeletonised visual hulls reconstructed from multi-view video. The pose is estimated independently in each frame, so the method can recover from errors in previous frames, which overcomes the problems of tracking. Publically available datasets were used to evaluate the method. On real data the method performs at a framerate of 15–64 fps depending on the resolution of the volume. Using synthetic data the positions of the extremities were determined with a mean error of 47–53 mm depending on the resolution.

1 INTRODUCTION

Capturing the motion of a person is a difficult task with a number of useful applications. Motion capture is used to identify people by their gait, for interacting with computers using gestures, for improving the performance of athletes, for diagnosis of orthopedic patients, and for creating virtual characters with more natural looking motions in movies and games. These are but a few of the possible applications of human motion capture.

In some of the application areas mentioned above it is important that the data aquisition is unconstrained by the markers or wearable sensors tradionally used in commercial motion capture systems. Furthermore, there is a need for low latency and real-time performance in some applications, for instance in perceptive user interfaces and gait recognition.

Computer vision based motion capture has been a highly active field of research in the last couple of decades, as surveys by for instance (Moeslund et al., 2006) and (Poppe, 2007) show. A popular approach for multi-camera setups has been the shape-from-silhouette method, which consists of doing 3D reconstruction from silhouette images that results in an over-estimate of the volume occupied by the subject called a visual hull.

Human motion is governed by an underlying articulated skeletal structure and (Moeslund et al., 2006) define pose estimation as the process of finding an approximate configuration of this structure in one or more frames. In a tracking framework the temporal relations between body parts during the motion sequence are ascertained. Many tracking based algorithms suffer from increasing errors over time, and recovering from situations where the track is lost can be problematic.

Goal. The overall goal of the research presented in this paper is to develop a robust, real-time pose estimation method.

Contribution. We present a pose estimation method based on constructing a tree structure from a skeletonised visual hull. The configuration of the skeletal structure is independently estimated in each frame, which overcomes limitations of tracking, and facilitates automatic initialisation and recovery from erroneous estimates. The method achieves real-time performance on a variety of different motion sequences.

This paper is organised as follows: in section 2 relevant work by other researchers is examined. The proposed pose estimation method is detailed in section 3. Results of experiments with the proposed method are presented in section 4, and the strengths and limitations of the approach are discussed in section 5. Section 6 concludes the paper.

Havnung Bakken R. and Hilton A..
REAL-TIME POSE ESTIMATION USING TREE STRUCTURES BUILT FROM SKELETONISED VOLUME SEQUENCES.
DOI: 10.5220/0003858501810190
In *Proceedings of the International Conference on Computer Vision Theory and Applications* (VISAPP-2012), pages 181-190
ISBN: 978-989-8565-04-4

2 RELATED WORK

The motion of the human body is governed by the skeleton, a rigid, articulated structure. Recovering this structure from image evidence is a common approach in computer vision based motion capture. Representing 3D objects by a skeletal approximation has many different applications. An overview of the properties, applications and algorithms for finding skeletal representations of 3D objects was given by (Cornea et al., 2007). There are several ways to define the skeletal representation of an object. The well-known medial axis transform (Blum, 1967) is used to thin objects in 2D, but when generalised to 3D it results in a medial surface. The skeleton of an object is defined as the locus of centre points of maximal inscribed balls. The medial axis and the skeleton are closely related, but not exactly the same. The curve-skeleton (Svensson et al., 2002) is an alternate representation without a rigorous definition, but generally it can be said to be a line-like 1D structure consisting of curves that match the topology of the 3D object.

There exists a plethora of algorithms for finding the curve-skeleton of an object, but (Cornea et al., 2007) divides them into four broad categories: thinning, geometrical, distance field, and potential field. A thorough discussion of the strengths and weaknesses of each type of approach is beyond the scope of this paper, but thinning offers a good compromise between accuracy and computational cost. A subset of the thinning category consists of fully parallel algorithms. These procedures evaluate each voxel of the 3D object independently, making them very well suited for implementation on modern graphics hardware.

Both (Brostow et al., 2004) and (Theobalt et al., 2004) sought to find the skeletal articulation of arbitrary moving subjects. Both approaches enforce temporal consistency for the entire structure during the motion sequence. Neither focused on human pose estimation specifically, however, and no inferences were made about which part of the extracted skeletons correspond to limbs in a human skeletal structure.

A method for automatic initialisation based on homeomorphic alignment of a data skeleton with a weighted model tree was presented by (Raynal et al., 2010). The alignment was done by minimising the edit distance between the data and model trees. The method was intended to be used as an initialisation step for a pose estimation or tracking framework.

In the model-free motion capture method proposed by (Chu et al., 2003) volume sequences are transformed into a pose-invariant intrinsic space, removing pose-dependent nonlinearities. Principal curves in the intrinsic space are then projected back into Euclidean space to form a skeleton representation of the subject. This approach requires three passes through a pre-recorded volume sequence, hence it was not suited for real-time applications.

Fitting a kinematic model to the skeletal data is an approach taken by several researchers. The pose estimation framework described by (Moschini and Fusiello, 2009) used the hierarchical iterative closest point algorithm to fit a stick figure model to a set of data points on the skeleton curve. The method can recover from errors in matching, but requires manual initialisation. The approach presented by (Menier et al., 2006) uses Delauney triangulation to extract a set of skeleton points from a closed surface visual hull representation. A generative skeletal model is fitted to the data skeleton points using maximum a posteriori estimation. The method is fairly robust, even for sequences with fast motion. A tracking and pose estimation framework where Laplacian Eigenmaps were used to segment voxel data and extract a skeletal structure consisting of spline curves was presented by (Sundaresan and Chellappa, 2008). Common for the three aforementioned approaches is that they do not achieve real-time performance.

A comparison of real-time pose estimation methods was presented by (Michoud et al., 2007). Their findings were that real-time initialisation was a feature lacking from other approaches. Michoud et al.'s own approach has automatic initialisation and estimates pose with a framerate of around 30 fps. It does, however, rely on finding skin-coloured blobs in the visual hull to identify the face and hands, and this places restrictions on the clothing of the subject and the start pose, as well as requiring the camera system to be colour calibrated.

The real-time tracking framework presented by (Caillette et al., 2008) used variable length Markov models. Basic motion patterns were extracted from training sequences and used to train the classifier. The method includes automatic initialisation and some degree of recovery from errors, but as with all training based approaches it is sensitive to over-fitting to the training data, and recognition is limitied by the types of motion that was used during the training phase.

3 APPROACH

In this section, we will detail the steps in the proposed pose estimation method, starting with the input data, and ending up with a set of labelled trees representing the subject's pose during the motion sequence.

Table 1: Ratios of limb lengths in relation to the longest path in the skeleton from one hand to one foot.

Bone	Ratio	Bone	Ratio
Head	0.042	Upper spine	0.050
Upper neck	0.042	Lower spine	0.050
Lower neck	0.042	Hip	0.061
Shoulder	0.085	Thigh	0.172
Upper arm	0.124	Lower leg	0.184
Lower arm	0.121	Foot	0.050
Hand	0.029	Toe	0.025
Thorax	0.050		

3.1 Anthropometric Measurements

In a fashion similar to (Chen and Chai, 2009) we build a model of the human skeleton by parsing the data in the CMU motion capture database (`mocap.cs.cmu.edu`). The CMU database contains 2605 motion capture sequences of 144 subjects. For each sequence the performer is described by an Acclaim skeleton file that contains estimated bone lengths for 30 bones. We parse all the skeleton files in the database and calculate the mean bone lengths for a subset of the bones.

The stature was used as the reference length when calculating anthromopometric ratios by (Michoud et al., 2007), but as we wish to use these ratios before the tree is labelled it is unknown which parts of the tree constitute the stature. Hence, we need an alternative reference length. We observe that the longest path in the ideal tree structure in figure 1 is from one hand to one foot (since the tree is symmetric it does not matter which we choose). Consequently, we use the longest path in the tree as the reference length and it corresponds to the sum of the lengths of the hand, lower and upper arm, thorax, lower and upper spine, hip, thigh, lower leg, foot, and toe. We calculate the ratios for all limbs in relation to this longest path. The limb length ratios are shown in table 1.

3.2 3D Reconstruction and Skeletonisation

The first step in a shape-from-silhouette based approach is to separate foreground (subject) from background (everything else) in the image data. Both the real and synthetic data used in this paper comes with silhouette images already provided, so this step is not included in the method, nor in the processing times presented in section 4. There are, however, real-time background subtraction algorithms available that could be used. Any of the three methods examined by (Fauske et al., 2009) achieve real-time performance with reasonable segmentation results.

We assume that the camera system used is calibrated and synchronised. Experiments with multi-camera systems by (Starck et al., 2009) demonstrated that using eight or more cameras ensures good results from the 3D reconstruction phase.

Once the silhouettes have been extracted the calibration information from the cameras can be used to perform a 3D reconstruction. The silhouette images are cross sections of generalised cones with apexes in the focal points of the cameras. The visual hull (Laurentini, 1994) is created by intersecting the silhouette cones. Visual hulls can be represented by surfaces or volumes. We employ a simple algorithm that produces a volumetric visual hull. For all voxels in a regular grid we project that voxel's centre into each image plane and check if the projected point is inside or outside the silhouette. Voxels that have projected points inside all the silhouettes are kept and the rest are discarded. This procedure lacks the robustness associated with more advanced techniques, but its simplicity makes it attractive for implementation on graphics hardware.

A parallel thinning technique (Bertrand and Couprie, 2006) is used to skeletonise the visual hull. The algorithm is implemented on graphics hardware to achieve high throughput.

3.3 Pose Tree Construction

It is natural to represent the human body using a tree structure. The head, torso and limbs form a tree-like hierarchy. If the nodes in the tree are given positions in Euclidean space the tree describes a unique pose.

3.3.1 Main Algorithm

An overview of the method can be seen in algorithm 1. The first step is to create a tree structure from the skeleleton voxels. A node is created for each voxel, and neighbouring nodes are connected with edges. Next, the extremities (hands, feet, and head) are identified in the tree by first pruning away erroneous branches, and then examining branch lengths. The third step consists of using the identified extremity nodes to segment the tree into body parts (arms, legs, torso, and neck). Finally, a vector pointing forward is estimated and used to label the hands and feet as left or right. Further details about each step of the method are given in the following sections.

3.3.2 Building the Tree

The skeleton voxel data is traversed in a breadth-first manner to build the pose tree. We place the root of the tree in the top-most voxel. The nodes are placed

in a queue as they are created. When the first node in the queue is removed the neighours of that node's corresponding voxel is checked and new child nodes are added to the tree if those neighbours have not been visited before. This is repeated until the queue is empty. At this point all voxels connected to the top-most voxel will have been processed and given corresponding nodes in the tree.

3.3.3 Finding Extremities

The next step is to identify the extremities among the leaf nodes in the tree. The input skeleton voxels typically contain some noise which in turn leads to spurious branches in the tree. Hence, we need to prune the tree to reduce the number of leaf nodes. This is done in two steps. First, a recursive procedure that removes branches shorter than a threshold based on the anthropometric ratios is employed. Calculating the length of an arm with the anthropometric ratios from section 3.1 and using that as the threshold has been found to produce good results. Of the remaining leaf nodes the feet should be at the end of the two longest branches, and the hands should be at the end of the next two. Hence, the list of leaf nodes is sorted by branch length and all but the longest four are removed. In order to keep all information in the original tree intact the two pruning steps are performed on a copy.

The procedure outlined above is robust as long as the top-most voxel is at the location of the head. The head branch is shorter than the length of an arm and if one of the other limbs is higher than the head, the head branch is likely to be removed during pruning. We solve this problem by finding what we define as the *origin* node.

Algorithm 1: Main pose estimation algorithm

1: Build the pose tree from skeleton voxels.
2: Find the extremities (feet, hands, head).
3: Segment the tree into body parts.
4: Find a vector pointing forward, and identify left and right limbs.

Algorithm 2: A breadth-first pose tree construction algorithm.

```
1: Create a node for the top-most voxel and add it to the node queue.
2: while node queue is not empty do
3:    N ← first node in queue.
4:    V ← voxel corresponding to N.
5:    for all neighbours of V do
6:       if neighbour has not been visited then
7:          Create a new child node of N and add it to the queue.
8:          Label neighbour as visited.
9:       end if
10:   end for
11: end while
```

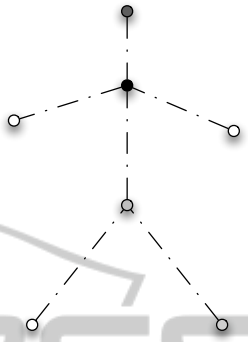

Figure 1: An ideal pose tree. The black node is the origin with degree four, the dark grey node is the root, the light grey node is the internal node of degree three, and the white nodes are leaf nodes. All other nodes are internal nodes of degree two.

Let us consider an ideal pose tree. An ideal pose tree consists of a root node, four leaf nodes, one internal node of degree three, one internal node of degree four, and a number of internal nodes of degree two as shown in figure 1. We define the origin node as the node of degree four where the arms, torso, and neck are joined.

All nodes in the pruned tree of degree higher than two are candidates for the origin node. In order to choose the best candidate we create copies of the pruned tree and move the root to each of the candidate locations. A rank is calculated for each of the candidate trees, and the root of the highest ranked tree is chosen as the origin node.

The leaf nodes in the candidate tree are sorted by distance to the root. The furthest two are used as feet, the next two as hands, and the last as head. Ideal lengths for the legs, arms, neck, and torso (I_l, I_a, I_n, I_t) are estimated using the anthropometric ratios and the longest path in the tree. We calculate the rank of a candidate using the following formula:

$$r = r_{l_1} \cdot r_{l_2} \cdot r_{a_1} \cdot r_{a_2} \cdot r_n \cdot e^{-\frac{(deg(root)-4)^2}{3}} \quad (1)$$

The last term is used to penalise candidate nodes with degree $\neq 4$. The ranks for each limb is given by the following formulae:

$$r_l = \frac{\min(I_l, d_r)}{\max(I_l, d_r)} \cdot \frac{\min(I_t, d_r - d_b)}{\max(I_t, d_r - d_b)} \quad (2)$$

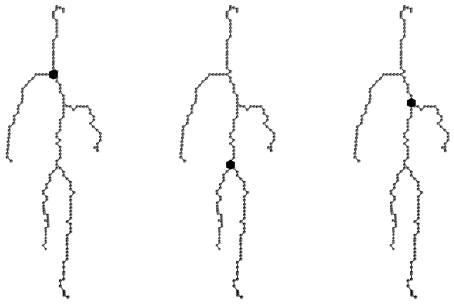

Figure 2: Three candidates for the origin node of a tree sorted by rank from left to right. Their ranks are 8.85×10^{-4}, 1.45×10^{-4}, and 3.40×10^{-5}, respectively.

$$r_a = \frac{\min(I_a, d_r)}{\max(I_a, d_r)} \cdot \frac{1}{1 + (d_r - d_b)} \quad (3)$$

$$r_n = \frac{\min(I_n, d_r)}{\max(I_n, d_r)} \cdot \frac{1}{1 + (d_r - d_b)} \quad (4)$$

where d_r is the distance from the leaf node under consideration to the root of the candidate tree, and d_b is the distance from the leaf node to the closest branching point. The second terms of equations 3 and 4 are used to penalise candidates where one arm has been shortened. An example of three candidate trees and their ranks can be seen in figure 2.

The root of the pruned copy of the pose tree is moved to the location of the highest ranked origin candidate. If this is the first frame or no valid labelling is available from the previous frame, the leaf nodes are sorted by the distance to the root. Finally, the nodes in the original pose tree corresponding to the remaining leaf nodes in the copy are labelled as extremities. The two furthest from the root are labelled as feet, the next two as hands, and the last one as the head.

If a valid labelling from the previous frame exists, we use temporal correspondences to label the extremities instead. For each of the labelled extremities in the previous frame, the Euclidean distance to each of the remaining candidates in the current frame is calculated and the one with the shortest distance is chosen. The chosen candidate is labelled correspondingly and removed from the list of candidates.

If the head node is not the root of the tree, the root is moved to that node. A lower limit on the origin node rank is used to determine the validity of the labelling. This threshold is set empirically, and if none of the candidate trees has a rank above the threshold the labelling is not considered valid, and will not be used for finding temporal correspondences in the next frame.

Algorithm 3: Finding extremities in the pose tree.

1: Create a copy of the tree.
2: Prune the copy by recursively removing branches that are shorter than an arm.
3: Examine the remaining leaf nodes, and remove all but the four belonging the longest branches (feet and hands).
4: Create copies of the pruned tree with candidates for the origin node position.
5: Rank the candidate trees and move the root of the pruned copy to the location of the root of the candidate tree with the highest rank.
6: **if** no valid labelling from previous frame **then**
7: Sort leaf nodes by distance to root.
8: Label the furthest two as feet, the next two as hands, and the final as head.
9: **else**
10: Label the leaf nodes by finding the nearest correspondences from the previous frame.
11: **end if**

3.3.4 Segmentation into Body Parts

Next, we segment the tree into body parts. The identified extremities are used as starting points for the segmentation. Starting in the first hand node, the tree is labelled as *Arm1* upwards until the root is reached. This is repeated for the other hand, and the tree is labelled as *Arm2* upwards until the first node labelled *Arm1* is encountered. Labelling continues upwards, and all nodes are labelled as *Neck* until the root is reached. A similar approach is used for the lower body. Starting in the first foot, the nodes are labelled as *Leg1* upwards in the tree until the label *Neck* is reached. From the second foot, the nodes are labelled as *Leg2* upwards in the tree until the label *Leg1* is encountered. Finally, continuing upwards, all nodes are labelled as *Torso* until the label *Neck* is encountered. If no nodes are labelled as *Torso*, the tree is marked as invalid. This procedure is formalised in algorithm 4.

Algorithm 4: Tree segmentation (arms only; the legs, neck, and torso are identified in a similar manner).

1: $N \leftarrow$ the leaf node labelled $Hand1$.
2: **while** N is not the root **do**
3: Label N as $Arm1$.
4: $N \leftarrow N$'s parent.
5: **end while**
6: $N \leftarrow$ the leaf node labelled $Hand2$.
7: **while** N is not labelled $Arm1$ **do**
8: Label N as $Arm2$.
9: $N \leftarrow N$'s parent.
10: **end while**
11: {Repeat for legs, neck and torso.}

3.3.5 Identifying Left and Right

The final step of the proposed method is to find the left and right sides of the body. We use the labelled extremities as the starting point. Using the anthropometric ratios from section 3.1 the algorithm creates sets of nodes corresponding to the feet, lower legs, thighs, and torso by traversing the tree upwards from the labelled leaf nodes. Total least squares line fitting is used to find vectors representing the node sets, while making sure all vectors point upwards in the tree.

Taking the cross products of the vectors, normal vectors for the ankle and joints are calculated. In figure 3(a) we observe that the angles α and β can never exceed 180°, so ordering the vectors in the cross-product consistently ensures that the normals will be oriented towards the left. For each leg the two joint normals are combined to form a normal for the leg, and a forward pointing vector for each leg is created by taking the cross product of the normals and the torso vector. The two forward vectors are combined to form a single vector pointing forward in the torso's frame of reference. This procedure is formalised in algorithm 5. Because of noise in the data it is possible that the foot can degenerate during the skeletonisation and tree construction phases. In order to avoid problems with the node sets used for the curve fitting, a threshold is set on the difference in length between the legs. If one leg is shorter by more than two times the length of a foot, the foot vector and consequently the ankle joint is disregarded in the calculation of the normals.

To label the hands as left and right, total least squares line fitting is used to find vectors representing the shoulders, both pointing away from the torso. A vector pointing left is calculated using the cross product of the torso vector with the forward vector. The angles between the shoulder vectors and the left vector is calculated, and the hand corresponding to the smallest angle is labelled as left. If both shoulder vectors are pointing in the same or opposite direction of the left vector, the largest and smallest angle with the forward vector, respectively, are used to label the left hand. The procedure is repeated for the feet using vectors representing the hips. The left-right labelling is formalised in algorithm 6.

4 RESULTS

A number of experiments have been conducted using the proposed method. Both real and synthetic data were used, and reconstructions were done at resolutions of $64 \times 64 \times 64$ and $128 \times 128 \times 128$ voxels. The sizes of a voxel were 31.3 mm at $64 \times 64 \times 64$, and 15.6 mm at $128 \times 128 \times 128$. All experiments were conducted on a computer with a 2.67 GHz Intel i7

Algorithm 5: Finding forward vector.

1: Using anthropometric ratios, create sets of nodes corresponding to the foot, lower leg, thigh, and torso.
2: Using orthogonal distance regression, fit lines to the sets of nodes, and make sure the resulting vectors $\vec{v}_{foot}, \vec{v}_{lleg}, \vec{v}_{thigh}, \vec{v}_{torso}$ point upwards in the tree.
3: **if** angle$(\vec{v}_{foot}, \vec{v}_{lleg}) > threshold$ **then**
4: Construct a normal for the ankle joint $\vec{n}_{ankle} = \vec{v}_{foot} \times \vec{v}_{lleg}$.
5: **end if**
6: **if** angle$(\vec{v}_{lleg}, \vec{v}_{thigh}) > threshold$ **then**
7: Construct a normal for the knee joint $\vec{n}_{knee} = \vec{v}_{lleg} \times -\vec{v}_{thigh}$.
8: **end if**
9: Combine the joint normals $\vec{n}_1 = \dfrac{\vec{n}_{ankle} + \vec{n}_{knee}}{|\vec{n}_{ankle} + \vec{n}_{knee}|}$.
10: Repeat step 3 to 9 for the other leg, to get a second normal n_2.
11: Construct two forward vectors using the normals $\vec{f}_1 = \vec{n}_1 \times \vec{v}_{torso}$.
12: Combine the two forward vectors $\vec{f} = \dfrac{\vec{f}_1 + \vec{f}_2}{|\vec{f}_1 + \vec{f}_2|}$.

Algorithm 6: Identifying left and right limbs.

1: For each arm, create a set of n nodes representing the shoulder.
2: Construct a vector pointing left $\vec{v}_{left} = \vec{v}_{torso} \times \vec{f}$
3: Using orthogonal distance regression, fit lines to the sets of nodes, and make sure the resulting vectors $\vec{v}_1$ and $\vec{v}_2$ point away from the torso.
4: **if** $\vec{v}_{left} \cdot \vec{v}_1 > 0$ and $\vec{v}_{left} \cdot \vec{v}_2 > 0$ **then**
5: $left = \arg\max(\text{angle}(\vec{f}, \vec{v}_1), \text{angle}(\vec{f}, \vec{v}_2))$
6: $right = \arg\min(\text{angle}(\vec{f}, \vec{v}_1), \text{angle}(\vec{f}, \vec{v}_2))$
7: **else if** $\vec{v}_{left} \cdot \vec{v}_1 < 0$ and $\vec{v}_{left} \cdot \vec{v}_2 < 0$ **then**
8: $left = \arg\min(\text{angle}(\vec{f}, \vec{v}_1), \text{angle}(\vec{f}, \vec{v}_2))$
9: $right = \arg\max(\text{angle}(\vec{f}, \vec{v}_1), \text{angle}(\vec{f}, \vec{v}_2))$
10: **else**
11: $left = \arg\min(\text{angle}(\vec{v}_{left}, \vec{v}_1), \text{angle}(\vec{v}_{left}, \vec{v}_2))$
12: $right = \arg\max(\text{angle}(\vec{v}_{left}, \vec{v}_1), \text{angle}(\vec{v}_{left}, \vec{v}_2))$
13: **end if**
14: For each leg, create a set of n nodes representing the hip, and repeat steps 3 to 12.

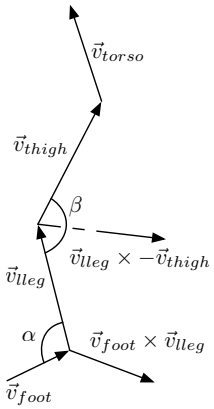

(a) Joint angles and normals.

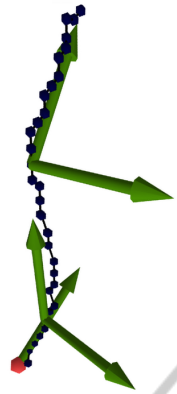

(b) Example using real data.

Figure 3: Vectors used for left-right labelling.

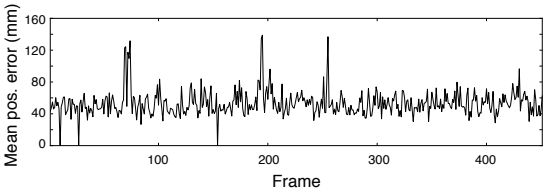

(a) Volume resolution $64 \times 64 \times 64$.

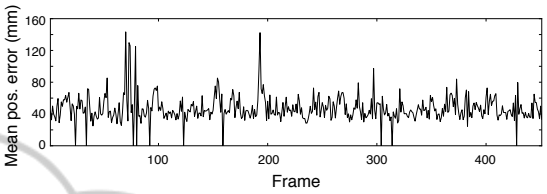

(b) Volume resolution $128 \times 128 \times 128$.

Figure 4: Comparison of mean errors of estimated positions of the hands and feet for a synthetic dance sequence. Frames where the algorithm has failed gracefully have been omitted.

processor, 12 GB RAM, and two graphics cards: one Nvidia GeForce GTX 295 and one Nvidia GeForce GTX 560 Ti. The GTX 295 was used for visual hull construction and the GTX 560 for skeletonisation.

The accuracy of the method at different volume resolutions was evaluated using synthetic data. An avatar was animated using motion capture data from the CMU dataset. Silhouette images of the sequence were rendered with eight virtual cameras at a resolution of 800×600, seven placed around the avatar and one in the ceiling pointing down. The sequence that was used was a whirling dance motion (subject 55, trial 1). The known joint locations from the motion capture data were used as a basis for comparison. The results of using the proposed pose estimation method on the synthetic data can be seen in figure 4. The mean positional error of the hands and feet for the entire sequence was 46.8 mm (standard deviation 16.6 mm) and 53.2 mm (standard deviation 15.9 mm) for $128 \times 128 \times 128$ and $64 \times 64 \times 64$ volume resolutions, respectively. There is a noticeable increase in accuracy with a higher resolution, but not by a huge margin. An interesting observation is that the number of frames where the method fails (curve reaches 0) increases with higher resolution. The sequence consists of 451 frames, and 97.6% and 95.8% are labelled correctly at $64 \times 64 \times 64$ and $128 \times 128 \times 128$ resolutions, respectively.

The robustness and computational cost of the method was evaluated using real data drawn from the i3DPost dataset (Gkalelis et al., 2009). This is a publically available multi-view video dataset of a range of different motions captured in a studio environment. The volume resolution greatly influences the processing time of the method. Three sequences of varying complexity were tested at both $64 \times 64 \times 64$ and $128 \times 128 \times 128$ resolutions, and the results can be seen in table 2. The method achieves near real-time performance of ~ 15 fps at the highest resolution, but by halving the dimensions of the volume the framerate is almost tripled. A framerate of ~ 64 fps should be sufficient for most real-time applications. In both cases the tree construction is highly efficient, < 1.5 ms for $64 \times 64 \times 64$ and < 4 ms for $128 \times 128 \times 128$. At the higher resolution the skeletonisation is the main computational bottleneck. The reason for the small difference in processing time for the visual hull construction is that the images from the i3DPost dataset have a resolution of 1920×1080 and copying the data between main memory and the GPU is the bottleneck. Figure 5 shows four frames from the three sequences at both resolutions.

Sequences with challenging motions were used to test the robustness. Poses where the subject's limbs are close to the body typically result in a visual hull that is a poorer approximation of the actual volume. A sequence where the subject is crouching during the motion illustrates this. As can be seen in figure 6 the method fails gracefully when the subject is crouching, but recovers once the limbs are spread out once more. A pirouette is a challenging motion, because of the rapid movement of the extremities. Figure 7 shows that the temporal correspondence labelling can fail in such cases, but the identification of the left and right limbs is still robust.

For the real data, the *walk* (57 frames) and *walk-spin* (46 frames) sequences are labelled 100% correctly. Only 42.6% of the *run-crouch-jump* (108 frames) sequence is labelled correctly, but the subject is crouching during half the sequence. The sequences

Table 2: Comparison of mean processing times for three sequences from the i3DPost dataset, using different resolutions. All times are in milliseconds, with standard deviations in parentheses.

(a) Volume resolution $64 \times 64 \times 64$.

	Visual hull	Skeletonisation	Build tree	Sum	Framerate
Walk, sequence 013	9.61 (0.26)	4.37 (0.28)	1.44 (0.25)	15.41 (0.47)	64.88
Walk-spin, sequence 015	9.63 (0.26)	4.42 (0.32)	1.41 (0.30)	15.46 (0.54)	64.67
Run-crouch-jump, sequence 017	9.69 (0.26)	4.82 (0.59)	1.07 (0.27)	15.58 (0.61)	64.18

(b) Volume resolution $128 \times 128 \times 128$.

	Visual hull	Skeletonisation	Build tree	Sum	Framerate
Walk, sequence 013	12.25 (0.34)	49.37 (2.63)	3.09 (0.33)	64.71 (2.61)	15.45
Walk-spin, sequence 015	12.28 (0.30)	52.06 (4.14)	3.13 (0.46)	67.46 (4.03)	14.82
Run-crouch-jump, sequence 017	11.94 (0.16)	51.43 (3.73)	3.51 (0.58)	66.88 (3.89)	14.95

(a) Walk, sequence 013.

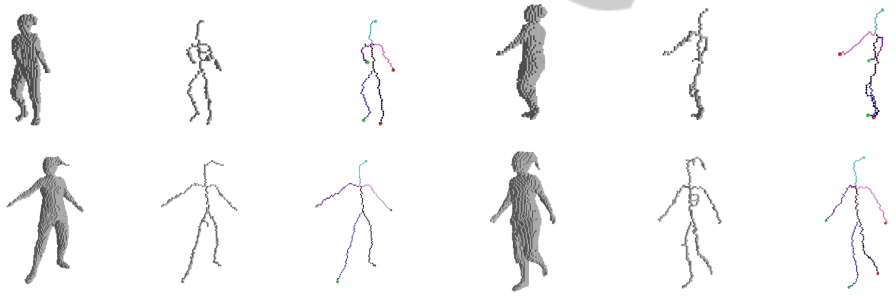

(b) Walk-spin, sequence 015.

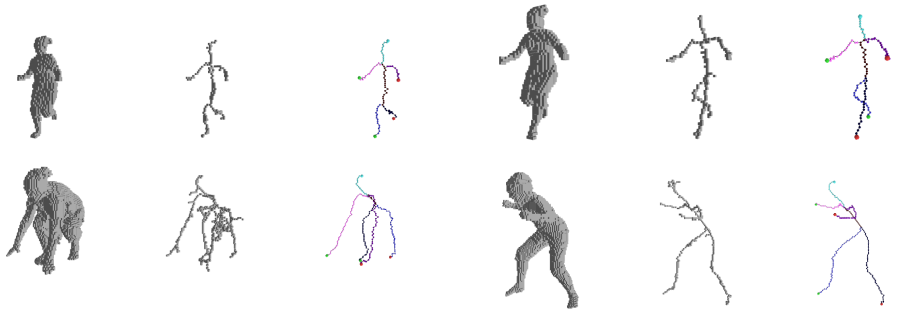

(c) Run-crouch-jump, sequence 017.

Figure 5: Four frames from each of three sequences, showing the visual hulls, skeletons and pose trees. The top rows have a volume resolution of $64 \times 64 \times 64$, and $128 \times 128 \times 128$ in the bottom rows.

Figure 6: Five frames from the run-crouch-jump sequence (017 from the i3DPost dataset) illustrating the problems that occur when the subject is crouching and no reliable skeleton can be extracted, but also that the algorithm recovers when the arms and legs become distinguishable again.

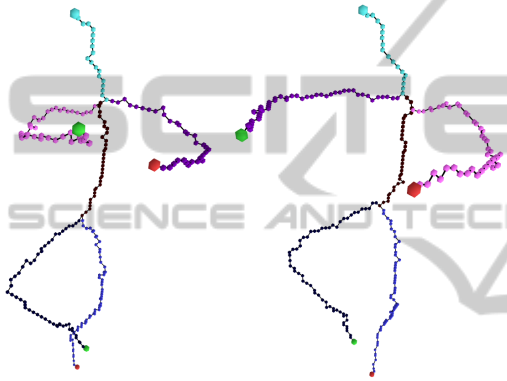

Figure 7: Two consecutive frames of a ballet sequence (023 of the i3DPost dataset) where the correspondence labelling has failed and the arm colours have switched sides. The left-right labelling, however, is still correct as illustrated by the red and green extremities.

were truncated to keep the subject completely inside the viewing volume. The *ballet* sequence consists of 150 frames and 87.3% of them were labelled correctly.

5 DISCUSSION AND FUTURE WORK

In the previous section we demonstrated the proposed method on several sequences where it robustly recovers a segmented skeletal structure. There are, however, some limitations to using a skeletonisation based approach, and we will discuss them here, and how these issues can be resolved in the future.

Cases can be found that are likely to be problematic for a skeletonisation based method. The extracted skeleton is unreliable in frames where the limbs are not clearly separated from the rest of the body. However, it is possible to detect these cases and give an indication that the pose estimate for that particular frame is not trustworthy. A significant advantage of the proposed approach is that the skeleton in each frame can be labelled independently of previous frames. As was demonstrated in section 4 this allows the approach to recover from errors in previous frames where the skeletal reconstruction may be degenerate.

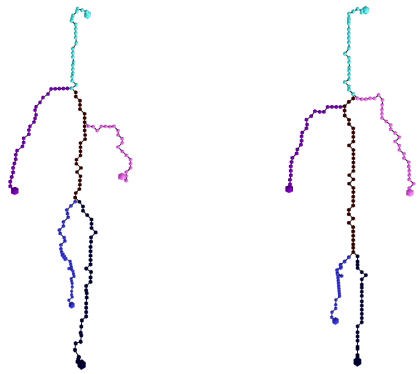

Figure 8: Two frames of a walk sequence (013 from the i3DPost dataset) demonstrating the possible displacement of the shoulders and the pelvis. The proposed method compensates for this, and the limbs are still labeled correctly.

In figure 8 we see a common problem with using the curve-skeleton. In frames where the arms are close to the torso or the legs are too close to each other, the shoulders and pelvis tend to be displaced downwards. This is not a major issue for the proposed algorithm, but it is important to keep in mind if more joint locations should be extracted in the future.

The lower limit on the rank of candidate trees we use to determine a labelling's validity is heuristic, and a better alternative should be found. Though the empirically set threshold works for the sequences we have tested with, there are no guarantees that it will do so for other data.

Currently, only the locations of the hands, feet, and the head are estimated. We intend to extend the method with estimates for the positions of internal joints as well. Creating a kinematic model using the limb length ratios in section 3.1 and fitting that to the skeleton data is an approach that will be examined further.

In order to better compare the proposed approach to other methods that attempt to solve the pose estimation problem, the method should be tested on more publically available datasets, for instance HumanEVA or INRIA IXMAS.

6 CONCLUDING REMARKS

We have presented a novel pose estimation method based on constructing tree structures from skeletonised sequences of visual hulls. The trees are pruned, segmented into body parts, and the extremities are identified. This is intended to be a real-time approach for pose estimation, the results for the pose tree computation back this up and demonstrate good labellings across multiple sequences with complex motion. The approach can recover from errors or degeneracies in the initial volume/skeletal reconstruction which overcomes inherent limitatons of many tracking approaches which cannot re-initialise. Ground-truth evaluation on synthetic data indicates correct extremity labelling in $\sim 95\%$ of frames with rms errors < 5 cm.

ACKNOWLEDGEMENTS

The authors wish to thank Lars M. Eliassen for helping with the implementation of the skeletonisation algorithm, and Odd Erik Gundersen for his helpful comments during the writing of the paper. Some of the data used in this project was obtained from mocap.cs.cmu.edu. The CMU database was created with funding from NSF EIA-0196217.

REFERENCES

Bertrand, G. and Couprie, M. (2006). A New 3D Parallel Thinning Scheme Based on Critical Kernels. *Discrete Geometry for Computer Imagery (LNCS)*, 4245:580–591.

Blum, H. (1967). A transformation for extracting new descriptors of shape. *Models for the perception of speech and visual form*, 19(5):362–380.

Brostow, G. J., Essa, I., Steedly, D., and Kwatra, V. (2004). Novel skeletal representation for articulated creatures. *Computer Vision - ECCV (LNCS)*, 3023:66–78.

Caillette, F., Galata, A., and Howard, T. (2008). Real-time 3-D human body tracking using learnt models of behaviour. *Computer Vision and Image Understanding*, 109(2):112–125.

Chen, Y.-l. and Chai, J. (2009). 3D Reconstruction of Human Motion and Skeleton from Uncalibrated Monocular Video. *Computer Vision - ACCV (LNCS)*, 5994:71–82.

Chu, C.-W., Jenkins, O. C., and Mataric, M. J. (2003). Markerless Kinematic Model and Motion Capture from Volume Sequences. In *Proceedings of the IEEE Conference on Computer Vision and Pattern Recognition*, pages 475–482.

Cornea, N. D., Silver, D., and Min, P. (2007). Curve-Skeleton Properties, Applications, and Algorithms. *IEEE Transactions on Visualization and Computer Graphics*, 13(3):530–548.

Fauske, E., Eliassen, L. M., and Bakken, R. H. (2009). A Comparison of Learning Based Background Subtraction Techniques Implemented in CUDA. In *Proceedings of the First Norwegian Artificial Intelligence Symposium*, pages 181–192.

Gkalelis, N., Kim, H., Hilton, A., Nikolaidis, N., and Pitas, I. (2009). The i3DPost multi-view and 3D human action/interaction database. In *Proceedings of the Conference for Visual Media Production*, pages 159–168.

Laurentini, A. (1994). The Visual Hull Concept for Silhouette-Based Image Understanding. *IEEE Transactions on Pattern Analysis and Machine Intelligence*, 16(2):150–162.

Menier, C., Boyer, E., and Raffin, B. (2006). 3D Skeleton-Based Body Pose Recovery. In *Proceedings of the Third International Symposium on 3D Data Processing, Visualization, and Transmission*, pages 389–396.

Michoud, B., Guillou, E., and Bouakaz, S. (2007). Real-time and markerless 3D human motion capture using multiple views. *Human Motion - Understanding, Modeling, Capture and Animation (LNCS)*, 4814:88–103.

Moeslund, T. B., Hilton, A., and Krüger, V. (2006). A survey of advances in vision-based human motion capture and analysis. *Computer Vision and Image Understanding*, 104:90–126.

Moschini, D. and Fusiello, A. (2009). Tracking Human Motion with Multiple Cameras Using an Articulated Model. *Computer Vision/Computer Graphics Collaboration Techniques (LNCS)*, 5496:1–12.

Poppe, R. (2007). Vision-based human motion analysis: An overview. *Computer Vision and Image Understanding*, 108(1-2):4–18.

Raynal, B., Couprie, M., and Nozick, V. (2010). Generic Initialization for Motion Capture from 3D Shape. *Image Analysis and Recognition (LNCS)*, 6111:306–315.

Starck, J., Maki, A., Nobuhara, S., Hilton, A., and Matsuyama, T. (2009). The Multiple-Camera 3-D Production Studio. *IEEE Transactions on Circuits and Systems for Video Technology*, 19(6):856–869.

Sundaresan, A. and Chellappa, R. (2008). Model-driven segmentation of articulating humans in Laplacian Eigenspace. *IEEE Transactions on Pattern Analysis and Machine Intelligence*, 30(10):1771–1785.

Svensson, S., Nyström, I., and Sanniti di Baja, G. (2002). Curve skeletonization of surface-like objects in 3D images guided by voxel classification. *Pattern Recognition Letters*, 23:1419–1426.

Theobalt, C., de Aguiar, E., Magnor, M. A., Theisel, H., and Seidel, H.-P. (2004). Marker-free kinematic skeleton estimation from sequences of volume data. *Proceedings of the ACM symposium on Virtual reality software and technology - VRST '04*, D:57.